ISBN: 978-3-95450-236-3 ISSN: 2673-5350 doi:10.18429/JACoW-IBIC2023-TU3C05

LOW INTENSITY BEAM CURRENT MEASUREMENT OF THE ASSOCIATED PROTON BEAM LINE AT CSNS

R.Y. Qiu, W.L. Huang, F. Li, L. Zeng, Muhammad Abdul Rehman, M.Y. Liu, Q.R. Liu, R.J. Yang, T. Yang, Z.H. Xu, Z.X. Tan
Institute of High Energy Physics, Chinese Academy of Sciences, Beijing, China
Spallation Neutron Source Science Center, Dongguan, China

Abstract

The Associated Proton beam Experiment Platform (APEP) beamline is the first proton irradiation facility to use naturally-stripped protons which come from H- beams interacting with the residual gas in the linac beampipe at CSNS. The stripped beam current, which is in the order of 0.1% of the original H- beam and approximately 10 microamperes, should be measured precisely to provide the proton number for irradiation experiments. Therefore, a low-intensity beam current measurement system was developed with considerations to eliminate the external interferences. An anti-interference design is adopted in this system with an elaboration of probes, cables and electronic low-noise technology to minimize the impact of environmental noise and interferences. This improves the signal-to-noise ratio and enables a more precise measurement of the microampere-level pulsed beam current. The system was installed and tested during the summer maintenance in 2021 and 2022. It shows a good agreement with the measurement of the Faraday cup.

INTRODUCTION

The linear accelerator of China Spallation Neutron Source (CSNS) consists of a negative hydrogen ion source, a 3 MeV radio frequency quadrupole accelerator (RFQ), and a 4-tank drift tube linear accelerator (DTL) [1]. The negative hydrogen ion beam is accelerated to 80 MeV and then injected into the Rapid Cycling Synchrotron (RCS) by charge-exchange stripping. The proton beam is then accelerated to 1.6 GeV and finally extracted to bombard the tungsten target for neutron production with a repetition rate of 25 Hz [3]. In the linac of CSNS, a portion of H- beam interacts with the residual gas. As a result, in the beampipe there are three types of particles with different charge states: H^- (~15 mA, 100~500 μs), hydrogen atom (H^0), and proton (H^+). The associated proton beam current is about 0.1% of the original H^- beam. Therefore, the APEP beam line is established from the bending magnet at the end of linac. The number of protons in the beam is a crucial parameter for irradiation experiments.

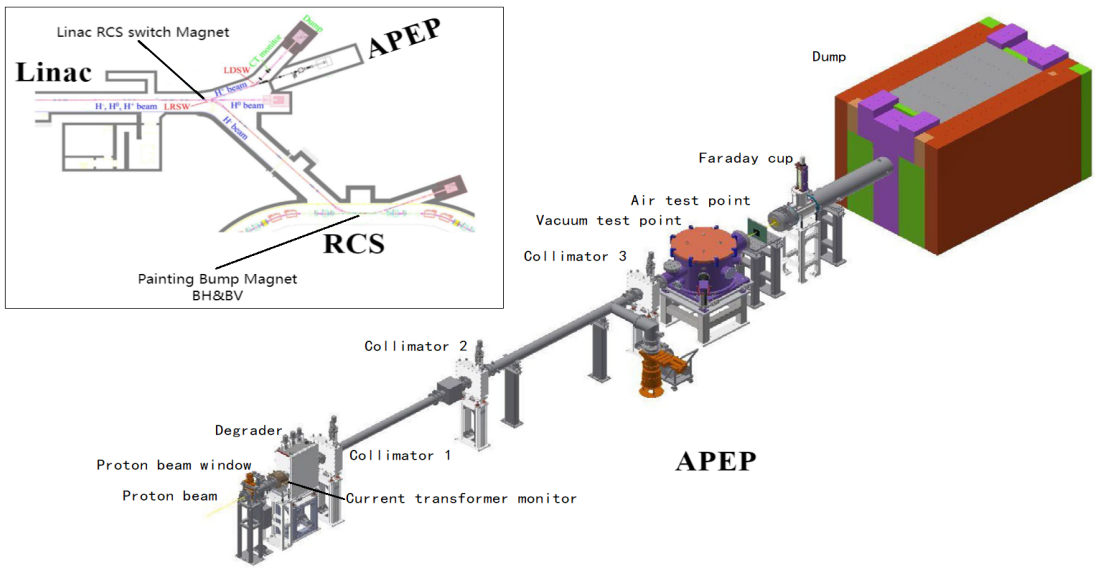

Figure 1: Layout of the APEP beam line. [2].

Figure 1 shows the layout diagram of the APEP area. There are three devices used for measuring beam intensity. The first one is the current transformer measurement system located at the entrance of APEP. In order to precisely measure this microampere-level beam intensity, a low-intensity beam current measurement system was developed in 2021. It achieved stable measurements by addressing external interferences in September 2022.The second device, located behind collimator3, is the beam intensity measurement system based on the secondary electron emission method. The third device is the Faraday cup beam intensity measurement device located in front of the DUMP. The two devices behind are currently undergoing debugging.

ISBN: 978-3-95450-236-3 ISSN: 2673-5350 doi:10.18429/JACoW-IBIC2023-TU3C05

This article primarily focuses on the design of the micro-ampere-level beam intensity measurement system for the beam current transformer.

Table 1: Parameters of the Associated Proton Beam

Parameter	Value
Proton Beam Energy	80 MeV
Repetition Frequency	25 Hz
Number of Particles	~5.0*10^{10} ppp@100 kW
Macro Bunch Length	100 μs ~ 500 μs
Proton Beam Intensity	20 μA@400 μs,100 kW

SYSTEM DESIGN

Design of Beam Current Detector

Before developing a current transformer, several soft magnetic alloy materials were tested and compared. Finally, an iron-based soft magnetic alloy core was selected due to its high magnetic permeability (μ_r), low coercivity (H_c), high saturation magnetic induction (B_s) and low cost. In the design of the transformer, it is necessary to consider that the droop of the 500 μs macro pulse signal should be less than 1% within the pulse width, that is, $\tau_{droop} > 0.05$ s or $f_{low\text{-}cutoff} = 7$ Hz. According to the measured noise level of the experiment, the turns of the secondary coil N_s was selected as 50. An additional coil of 1 turn was wound for the online calibration. Since the inner diameter of the vacuum pipeline is Φ110 mm, a soft magnetic core of Fe-based nanocrystalline alloy (nominal relative magnetic permeability $\mu_r \approx 90000$@10 Hz) with an inner diameter $D_i = 130$ mm, outer diameter $D_o = 160$ mm and longitudinal length $h = 25$ mm was selected for winding the current transformer. The equivalent inductance L_s of the sensor was calculated according to Eq. (1) as 0.175 H. It was measured by an LCR meter (HIOKI IM3536) to be 0.176 H@10 Hz, which is close to the theoretical calculation.

$$L_s = N_S{}^2 \frac{\mu_0 \mu_r f_{fill}}{2\pi} h \ln \frac{D_o}{D_i} \quad (1)$$

Here in Eq. (1): $\mu_0 = 4\pi \times 10^{-7}$ H/s is the vacuum magnetic permeability and $f_{fill} = 0.75$ is the filling factor of the ribbons forming the soft magnetic core. The input impedance of electronics r = 2.5 Ω, leads to the droop time constant of the pulse signal $\tau_{droop} = L_s/r = 0.062 > 0.05$ s, which meets the design requirements.

As shown in Fig. 1,the APEP current transformer is installed at the downstream of a bending magnet, which is used to guide the associated proton beam to the L-Dump or the APEP beam line. The stray magnetic field may cause the current transformer of APEP-CT to be magnetically saturated and fail to accurately measure the beam current strength of associated protons, so it is necessary to design a magnetic shield semi-surrounding the outside of the current transformer, as the inner shielding shown in Fig. 2. Considering the environmental stray magnetic field, a double-layered DT4 magnetic shield is designed according to Eq. (2). In this formula, $p=b^2/a^2$, where a and b are respectively the outer diameter and inner diameter of the cylindrical magnetic shield layer, and μ_r is the relevant permeability of magnetic material [4]. The magnetic shielding efficiency of a double-layered DT4 shield is calculated as a product of that of each layer with a radial thickness of 1 mm, that is, 37.8×38.7=1463, which is better than that of a single layer permalloy shield (S of which is 1220) with a radial thickness of 2.0 mm and a same outer diameter of Φ162 mm. The comparison of different magnetic shield is showed in Table 2. What's more, the material of DT4 is easy to process and costs much less. It can be seen that compared with a single-layer permalloy shield, this scheme has low cost and can meet the requirements of current transformers for magnetic shielding effect.

$$S = \frac{4\mu_r p}{(\mu_r^2+1)(p-1)+2\mu_r(p+1)} \quad (2)$$

Table 2: Calculation of Different Magnetic Shields as the Inner Shielding of APEP-CT

Layer Material	b mm	a mm	p	μ_r	S
DT4	162.0	160.0	1.0252	6000	37.8
DT4	158.0	156.0	1.0258	6000	38.7
Permalloy	162.0	158.0	1.0513	106	1220

A fully-enclosing outer shield of the APEP-CT sensor acts as a low-impedance path of the wall current and an RF shielding [5].

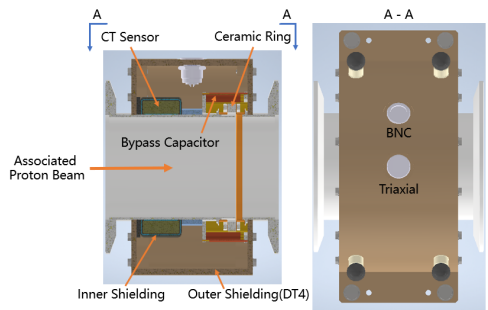

Figure 2: APEP CT sensor and magnetic shields.

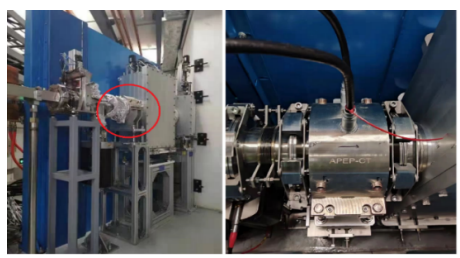

Figure 3: Proton beam intensity detector installed at the APEP tunnel.

Design of Electronic Circuit

As a current transformer, when the sensor detects the proton beam current, the induced output signal is a very weak current (here N_s=50). In the design of electronics, we use a transimpedance amplifier as the first-stage IV conversion chip. For instance, a 10 μA beam current passes through the sensor core with the 50-turn secondary coil, the input current of the electronics will be 200 nA. The input

ISBN: 978-3-95450-236-3 ISSN: 2673-5350 doi:10.18429/JACoW-IBIC2023-TU3C05

and feedback resistances of the electronics are r = 2.5 Ω and R_f = 10 kΩ * 20 separately. When selecting a low-noise operational amplifier, the input bias current I_b cannot be ignored. The bandwidth of the electronics should be designed to minimize high frequency noise introduction while meeting the rise time requirement. The circuit diagram is shown in Fig. 4. The electronic baseline is automatically adjusted by a technique of baseline dynamic feedback [6].

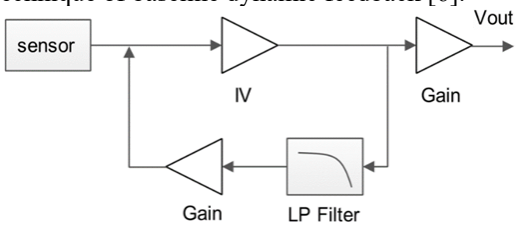

Figure 4: Diagram of CT electronics.

Experiments on Cable Selection and Shielding

We tested two kinds of cables to transport the signal from the sensor output to the electronics input. A comparison was made among the noise measurements of four-core cables (two-core twisted pair with braided outer shield) and triaxial cables under different grounding methods with the same sensor and electronics. It showed that the best signal-to-noise ratio was obtained when the triaxial cables were grounded at both ends. After the multi-point grounding test, it was found that outermost layer of triaxial cable was grounded to the vacuum pipeline at the sensor end, and the electronic end was grounded to cabinet ground to achieve the best effect, as shown in Fig. 5.

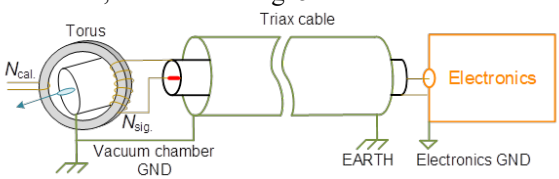

Figure 5: Diagram of the triax cable grounding to minimize noises.

SYSTEM CALIBRATION AND TESTING

System Calibration

We used a high precision pulsed current source Keithley 6221 to generate a current of square wave with a 500 μs pulse width in a range of 2~10 μA, which passed through the calibration coil of the APEP-CT sensor to simulate the beam current. The induced current in the secondary coil is input to the electronics via a 25 m triaxial cable and the electronics output voltage is measured by an oscilloscope or JYTEK DAQ for the data acquisition and waveform display. The calibration formula is obtained by a linear fitting of the electronic output amplitude with the simulated input beam current intensity. Through this formula, the undertest beam intensity can be calculated along with the background de-noising at a homo-metric beam-off zone during operation. Thereby we realized a precise low intensity measurement of the associated pulsed proton beam. After the system commissioning, the rise time of the electronics achieved < 10 μs, the droop time is < 1%/ms, and the relevant error of the calibration data is within 1% FS, as shown in Figs. 6 and 7. The parameters of this low intensity measurement system meet the design requirements.

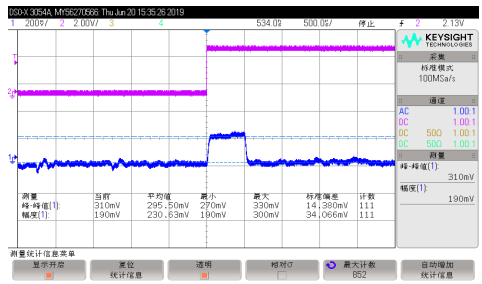

Figure 6: The blue signal is the electronics output with 1 μA calibrated input current.

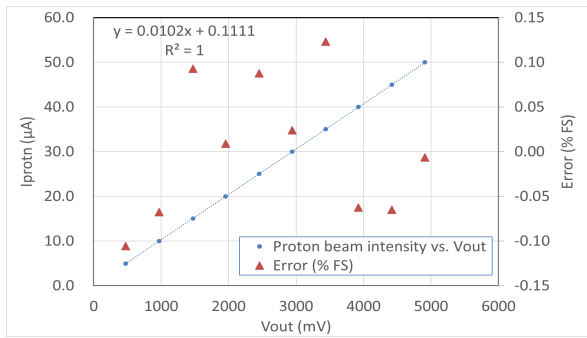

Figure 7: CT Electronics calibration data.

Troubleshooting and Experimentation for Interference Investigation

The low beam intensity measurement system was installed in the APEP tunnel during the summer maintenance in 2021. In the following accelerator operation, we performed several beam tests with this system, which needs guiding the beam to the APEP beamline. It performed abnormal due to significant interferences. The interference was large and stable, characterized by a fixed frequency relating to the beam current. A Faraday cup at the end of the APEP beam line detects the same interference signal, but with a relatively smaller impact, shown in Fig. 8.

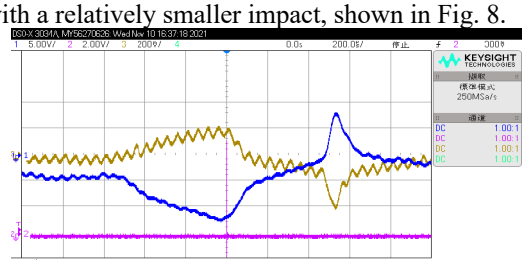

Figure 8: Measurement of the APEP-CT and Faraday cup electronic output waveforms. Blue trace is the signal of Faraday Cup. Yellow trace is that of APEP-CT. Purple trace is the timing trigger signal.

We made a thorough examination of the CT interference sources along the APEP beamline and RCS. The magnetic elements such as Linac RCS Switch Magnet, Painting Bump Magnet at the RCS injection zone, and Extraction Magnets at the extraction zone were sequentially shut

ISBN: 978-3-95450-236-3 ISSN: 2673-5350 doi:10.18429/JACoW-IBIC2023-TU3C05

down. The position of the magnet is shown in Fig. 1. The BH (Horizontal painting bump magnets) and BV (vertical painting bump magnets) are used for the horizontal and vertical painting respectively in the phase space of the injected beam. The main contribution of interference is from BH, followed by BV, which has a high similarity to the current curve of the power supply during the beam injection in the phase space painting mode. The correlation indicated that the interference was transmitted from the orbit bumper to the APEP-CT sensor along the accelerator vacuum pipe. The distance is about 55 meters. While other interference effects to the APEP-CT are small enough to be ignored.

Due to the consistent shape and amplitude of the interference signal, the DAQ system is triggered by the Timing system, allowing it to collect the interference signal once without a beam and save it as the background interference signal. Subsequently, for each subsequent signal collection with a beam, the interference signal is subtracted in order to restore the beam signal.

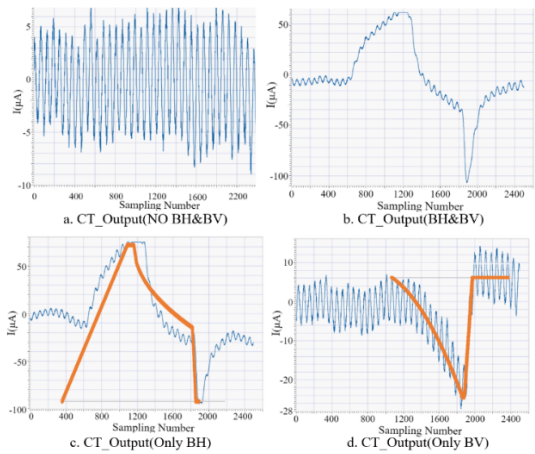

Figure 9: Output of APEP-CT electronics under different accelerator operation conditions. Pic (a) without BH and BV magnets operation. Pic (b) with the BH & BV magnet enabled. Pic (c) with only the BH magnet enabled. Pic (d) with only the BV magnet enabled.

To keep the interferences and high harmonics of the beam out of the sensor cavity, a bypass capacitor was designed (as shown in Fig. 2), and installed during the summer maintenance in 2022. The design principle of the bypass capacitor is described in Ref. [7]. The wall current splits in two: the high frequencies pass through the capacitance of the ceramic gap, which cancel the high frequency part of the beam "seen" by the sensor, and the low frequencies follow the wall current bypass, therefore do not pass through the sensor hole. Here, we built a capacitor over the ceramic gap with layers of copper foil separated by a layer of 100 μm-thick Kapton foil. The cavity impedance was dominated by the nanocrystalline core, which is measured to be 63.8 Ω@1 kHz and will be much bigger in higher frequencies. The bypass capacitance is designed as 5 nF, allowing the main part (<50 kHz) of the beam passing through the sensor hole. To obtain the desired capacitance value, the overlapping area is obtained by [8]:

$$S = {}^{C\,d}/_{\varepsilon_r \varepsilon_0} \qquad (3)$$

where: C is the capacitance [F],

$S = 1.61\times10^{-2}$ is the overlapping area [m^2],

$d = 1\times10^{-4}$ is the dielectric thickness [m],

ε_r is the relative dielectric constant, 3.5 for Kapton polyimid,

ε_0 is the dielectric constant 8.86 x 10^{-1}.

Figure 10: A bypass capacitor over the ceramic gap was built in the APEP-CT sensor.

Test Results

After the bypass capacitor was installed in the APEP-CT sensor, we successfully measured the associated proton beam in low intensity, shown in Fig.11. It was observed that the interference from the BH and BV magnets diminished significantly, and in fact, became barely noticeable. The signal-to-noise ratio of the beam signal was improved, and the amplitude of the pulsed associated proton beam intensity is clearly measured as 16.8 μA. The blue waveform represents the signal from the APEP-CT system, while the red waveform represents the current intensity signal measured by the Faraday cup after the beam passes through the energy degrader.

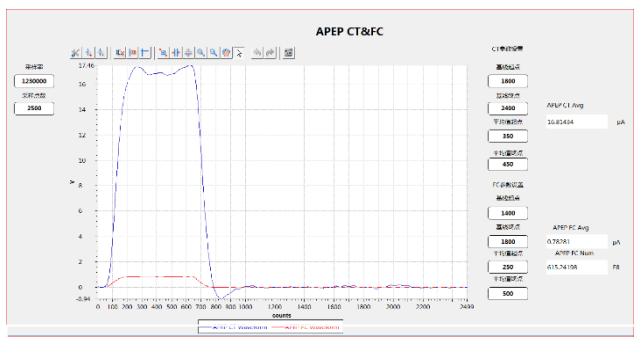

Figure 11: Output of the electronics of the APEP-CT and Faraday cup.

CONCLUSIONS

In the beam line of the Associated Proton beam Experiment Platform at CSNS, the proton beam intensity is a crucial parameter for irradiation experiments. The APEP-CT system achieves a signal-to-noise ratio improvement and meets the design specification for microampere-level current intensity measurement by implementing methods such as, the bypass capacitance design, the cable shielding and grounding methods, a low-noise electronic with the correct LP-filter design, and background noise subtraction algorithms in DAQ.

ISBN: 978-3-95450-236-3 ISSN: 2673-5350 doi:10.18429/JACoW-IBIC2023-TU3C05

REFERENCES

[1] S. Wang, Y. An, S. Fang *et al.*, "An overview of design for CSNS/RCS and beam transport," *Sci. China Phys. Mech. Astron,* vol. 54, no. 2, pp. 239–244, 2011. doi:10.1007/s11433-011-4564-x

[2] Yingyi Liu, Hantao Jing *et al.*, "Physical design of the APEP beam line at CSNS," *Nuclear Insrum. Methods Phys. Res. Sect. A,* vol. 1042, article id. 167431, 2022. doi:10.1016/j.nima.2022.167431

[3] S. Y. Xu, "Beam Commissioning Experience of CSNS/RCS", in *Proc. IPAC'19,* Melbourne, Australia, May 2019, pp. 1012-1014. doi:10.18429/JACoW-IPAC2019-MOPTS068

[4] G. Feng and Z. He, "Calculation and simulation of geomagnetic field shielding effectiveness of projectile body" [in Chinese], *Acta Metrologica Sin*., vol. 31, pp. 141-144, 2010. doi:10.3969/j.issn.1000-1158.2010.02.11

[5] Bergoz Instrumentation, *AC Current Transformer User's Manual*, Rev. 5.4, 2021.

[6] Q. Zhou and Z. Wang, "A DC-servo baseline restorer and its implementation in biomedical instrumentation", in *Proc. SPIE'06*, vol. 6040, pp. 320-325, 2005. doi:org/10.1117/12.664226

[7] W.L. Huang *et al.*, "A Dual Functional Current Monitor for Stripping Efficiency Measurement in CSNS", in *Proc. IBIC'19,* Malmö, Sweden, Sep. 2019, pp. 96-99. doi:10.18429/JACoW-IBIC2019-MOPP011

[8] Bergoz Instrumentation, *New Parametric Current Transformer User's Manual*, Rev. 1.1, 2014.